International Journal of Innovative Research in Science and Engineering
Volume 10, Issue 07, 2024
www.ijirse.com
ISSN: 2454-9665

Electrical Impedance Tomography: Transitioning from Conventional Architecture to the Innovative Field of Wearables

Mohd Faisal[1]

[1]*Research Scholar, Dept. of Computer Science & Engg.,*
College of Engineering & Technology
Bhagwant University Ajmer, Rajasthan, India
M_faisalcse@rediffmail.com

Dr. Pushpneel Verma[2]

[2]*Dept. of Computer science & Engg*
College of Engineering & Technology
Bhagwant Group of
Istitutions, Ajmer, Rajasthan, India.
pushpneelverma@gmail.com

Abstract:

Electrical impedance tomography (EIT) is a medical imaging technology that uses electrodes placed on the patient's skin to inject a current or voltage pattern. The electrodes then collect voltages, which are then used to rebuild the internal conductivity distribution of the patient.

EIT has several advantages over conventional imaging modalities, including excellent temporal resolution, non-invasiveness, and the absence of ionising radiation. Additionally, its great portability and inexpensive cost make it appropriate for bedside monitoring in real time.

Poor spatial resolution is a result of several technical restrictions that are also present in EIT. The ability to use EIT in the design of wearable devices has recently given this technology a boost. This paper reviewed the EIT physical foundations, hardware architecture, and significant clinical applications, ranging from traditional to wearable setups. A wearable, wireless EIT system appears to be a potential development in this field since it can enable new applications for EIT systems, such home monitoring, and make clinical measurements easier.

Keywords: wearable technology; electrical impedance tomography; imaging

1. Introduction

With the use of electrical stimulation and surface measurements, Electrical Impedance Tomography (EIT) is a real-time, radiation-free imaging method that reconstructs a subject's interior conductivity distribution. It is not a true tomographic technique, even if the traditional name was decided upon long ago, at the first Sheffield meeting in 1986. In fact, reassembling an image slice by slice is unfeasible due to the unconfined nature of low-

ISSN: 2454-9665

frequency electrical current, as any alteration in conductivity within the domain impacts all data, not just those on that particular slice [1].

EIT has various benefits as a medical imaging method. It is non-invasive, free of ionising radiation, has a high temporal resolution, and could be affordable. Its primary drawbacks include its poorer spatial resolution in comparison to other imaging modalities (echography, magnetic resonance imaging, and computed tomography), a high degree of inter-subject variability, artefacts from the movement of the electrodes, and poor contact quality. To increase picture resolution, many hardware options [2,3] and reconstruction techniques [4,5] have been put forth. EIT has a great deal of promise to be used in tandem with other imaging techniques to address many of their shortcomings, even though it can't yet match their high spatial resolution and precision. Furthermore, this technology has lately received a boost from the ability to construct wearable devices based on EIT, which might potentially represent a novel wearable imaging method.

A large number of review papers, such as general overviews [6], reviews of image reconstruction techniques [7], and works on clinical applications [8], have been published on EIT. With a focus on the advancements in hardware design from traditional systems to the most promising wearable implementations, this review paper seeks to provide a fresh perspective on this technology. Prior to presenting the traditional configuration of an EIT system and its primary application domains, the electrical characteristics of tissues are first explained. This is followed by a discussion of the stimulation approach, hardware implementation, and electrode design decisions. After that, the key characteristics of wearable EIT technology are examined, along with the most recent and pertinent wearables that have been documented in the literature.

The Biological impedance

Electric current can be impeded by living tissue, a property known as bioimpedance [9]. The electric resistance, or R, and the capacitive reactance, or X_C, are the real and imaginary components of a complex number that together make up bioimpedance.

$Z = R + jX_C$

Many studies have been conducted on the electrical characteristics of biological tissues in the literature [10], even relating them to physiological processes [11]. Cells floating in extracellular fluid make up biological tissues. Intracellular fluid is surrounded by a membrane in every cell. The extracellular and intracellular fluids offer resistive pathways and are very conductive. In addition to serving as a dielectric and supplying capacitive reactance, the lipid bilayer cell membrane divides the intracellular and external fluids.

The frequency of the applied electromagnetic field affects the tissues' electrical characteristics. Extracellular space is the primary conduit for current flow at low frequencies because to the high membrane impedance. Because of the long electrical route length caused by the current flowing around the cells, the medium's resistance rises. Higher frequencies cause the membrane's resistance to decrease, allowing current to pass through both the extracellular and intracellular media. The effective electrical path length decreases with increasing cross-sectional area through which current flows, lowering the medium's resistance. The impedance declines with frequency across the majority of frequency ranges, however dielectric dispersions, or plateaus, are scattered across the curve [12].

ISSN: 2454-9665

The bioimpedance of human tissues varies from about hundreds of Ω to hundreds of kΩ depending on their unique makeup. Large cells, a high concentration of extracellular water, a high number of cell connections, and a high cell content all lower resistance, whereas air, bone, and fat buildup raise impedance [13]. As a result, modifications to the physiological and pathological tissue composition also affect the regional bioimpedance [14]. When measuring tissue impedance, additional elements that may affect the electrical characteristics of the tissue, such as temperature, chemical and pH fluctuations, neuronal and muscle activation, and anisotropy dependance, must be taken into account [15, 16].

2. Imaging using Electrical Impedance Tomography

A low-intensity alternating current injected at the object boundary creates the surface potential, from which an EIT system reconstructs the bioimpedance map of a conducting domain. The following actions are needed for the system design:

• Select the imaging modality (differential or absolute), and specify the differential approach's reference dataset.
• Pick the right electrodes in terms of quantity, location, and substance.
• Specify the measuring approach (current-mode or voltage-mode).
• Create the electronic hardware, which includes the readout blocks for voltage and current generation.
• Select the numerical method for resolving the inverse problem.

The inverse problem, also known as the EIT problem, is a difficult one that involves reconstructing the impedance distribution from the applied current patterns and the observed electrode voltages. Image reconstruction is a very nonlocal and theoretically ill-posed issue in EIT since the current flow is dictated by the impedance distribution inside the object, as opposed to X-ray computed tomography, where the photons' pathways are straight lines [1]. It is important to emphasise that the current evaluation does not include the specifics of EIT reconstruction techniques. The literature has extensively examined potential solutions [7,17], along with several methods to boost resilience [18].

2.1. Imaging Modality of EIT

It is possible to use absolute or differential EIT imaging modalities [19]. In order to create a map of the absolute impedance, Absolute EIT needs a single experimental dataset. Although theoretically feasible, image reconstruction is not dependable in clinical settings due to many factors such as unclear boundary geometry, ambiguity surrounding electrode placements, and other sources of systematic artefacts [20].

As an alternative, differential EIT uses measurements of two datasets at different frequencies (frequency-difference EIT) or times (time-difference EIT) to create an image by detecting changes in impedance between the datasets. Errors in modelling and instrumentation are more resistant to this technique [21].

Time disparity EIT is an excellent tool for tracking physiological phenomena that change over time, however it is only useful in certain situations where time variation is present, including perfusion and lung ventilation. As an alternative, frequency-difference EIT allows for picture reconstruction in situations when time-referenced data are not available by measuring the various impedance characteristics of tissues at different measurement frequencies. However, its sensitivity is dependent on how the electrical frequency characteristics of the tissues

differ from one another, which might not be enough in some situations [22, 23]. Table 1 lists the various EIT imaging techniques along with their benefits and drawbacks.

Table 1: EIT imaging methods' benefits and drawbacks

Imaging Technique	**Output**	**Application**	**Advantages (+) and Disadvantages (−)**	
Absolute	Absolute impedance	Computer simulations	Always applicable Sensitive to instrumentation	modelling errors Not reliable in a clinical setting
Time-difference	Time-dependent impedance change	Time-varying phenomena	Robust to modelling errors	Time-referenced data required
Frequency-difference	Frequency-dependent impedance change	Identification of different tissues	Time-referenced data not required	Sufficient contact between tissues' electrical frequency properties required

2.2. Approaches to Measurement

Two methods are available for acquiring the signals: (1) voltage-mode EIT, which measures the induced currents after applying a known voltage to the tissue; (2) current-mode EIT, which measures the voltage produced on the body's surface after injecting a known current. Voltage-mode EIT devices exhibit a steady response across a large frequency range and are less expensive and easier to construct [24]. However, as current-mode EIT devices are easier to limit the maximum current injected to ensure system safety and are less susceptible to noise, they are typically chosen [24].

Current injection use several tactics based on the application:

• Adjacent method: Voltage is obtained between each of the remaining pairs of adjacent electrodes after current is injected between two adjacent electrodes. This is the method that is used the most [25].

• Polar or opposite method: Voltage is measured in pairs between the reference electrode and the remaining electrodes after current is injected between two electrodes spaced 180 degrees apart. This method is applied in the field of brain imaging [26].

• Cross or Diagonal method: In this method, one electrode is used as a reference for the voltage measurement, and current is injected between each pair of electrodes in turn. This process is repeated until all electrodes have been utilised as references. In EIT, this approach is not frequently employed [26].

- The trigonometric approach measures the voltage in relation to a reference electrode by injecting current into each electrode simultaneously. With the greatest number of independent measures guaranteed, this method is the one [25].

The conductivity and permittivity of the tissue being studied determine the frequency of the injected current [27]. The typical measuring frequency is 50 kHz, but in order to enhance image quality and examine various tissues, several instruments examine frequencies between 10 Hz and 10 MHz. High-performance circuit

components and data acquisition modules are necessary for frequencies above 1 MHz, as they can be difficult to achieve primarily because of parasitic impedances that distort the signals [24, 28].

2.3. The Electrode

The most important component of a bioimpedance measurement system is the electrode system, which stands for the electrochemical interface between the electronic system and the bodily tissue.

2.3.1 The Number

The quantity of electrodes to be employed is the first unresolved issue. While more independent measurements are available, increasing the number of electrodes improves image resolution but reduces precision and necessitates longer measurement and processing times [18]. Furthermore, contact impedance rises with the number of electrodes [25]. Although 16 electrodes is the most typical form, creative arrangements with up to 90 electrodes have been proposed for cancer detection [29]. For lung imaging applications, a greater number of electrodes—between 48 and 128 electrodes—is needed in 3D systems [30, 31]. Rotational EIT has been offered as a way to enhance the number of possible independent measurements without adding more electrodes: the electrodes are rotated to obtain more data. To accurately alter the electrode placements, a micro stepping motor [32] is used for the rotation. Positive outcomes have been attained [33], especially in the area of breast cancer detection [34].

2.3.2: Positioning

Also crucial to image reconstruction techniques is the electrode placement on the borders, which might result in a lack of resilience [18]. Because each electrode application requires a unique positioning, it might be challenging to establish standard placement on the human surface [35]. With wearable technology, this issue is exacerbated since non-specialized workers may apply or at the very least re-collocate a system. The time spent on manual positioning and the inter-operator variability are significantly decreased using a belt solution to address this issue [25]. A wearable system's inability to conform to varying body sizes may also be resolved by an elastic or adjustable electrode belt [36].

2.3.3: Impedance of Contact

Concerns of contact impedance exist in EIT as well. A decrease in the observed voltage at each electrode is the result of an electrochemical process that takes place at the electrode-skin interface. This process involves a change in the charge carriers, who are in charge of the current flow, at the interface between the metallic electrode and the body surface. Since body movement and surface conditions can affect contact impedance, it is typically high, unpredictable, and variable [35]. The reconstructed image may have flaws due to modelling mistakes that are not estimated or adjusted for [37]. A multi-pole measurement technique with four or more electrodes can be used to lessen the impact of contact impedance. This type of measurement yields a larger impedance of the measuring device in comparison to contact impedances [38].

Also, the capacitively coupled EIT approach (CCEIT), which creates a voltage excitation by a capacitive coupling, has been recently introduced as a contactless solution [40].

Furthermore, a novel contactless approach, the capacitively coupled EIT technique (CCEIT), has been recently introduced. It works by inducing a voltage excitation through a capacitive connection [40].

2.3.4 Sources of Interference

Additionally, a high contact impedance indicates that all types of interference, including crosstalk between cables, common mode gain error, thermal noise, and electromagnetic interference, reduce image resolution [35]. Active electrode-based EIT systems, which have each active electrode equipped with a separate signal conditioning circuit to lower input impedance, have been presented as a solution to this problem. In addition to lowering input impedance, this architecture has other benefits such as decreased susceptibility to electromagnetic interference and fewer cables required between the patient and the main electronics, which together make the system more comfortable [30,35,41–44].

2.3.5. Contacts

Since the electrodes are frequently positioned on pliable tissue in biomedical applications, making sure there is good contact is also essential [18]. Commonly used electrodes are adhesive Ag/AgCl with conductive gel. Volume electrodes may provide a safer contact, but their size and invasiveness are limited to reduce the risk of skin damage from injected current [18].

Another option would be to employ a defective contact detector algorithm [45], which would identify damaged electrodes so that staff could replace them and ensure adequate image reconstruction even in the case of partial detachments.

2.3.6. Wearable EIT Requirements

For wearable applications, maintaining a strong contact for extended periods of time and while moving is a special necessity. As wearables are often wireless and non-invasive, they are actually appropriate for long-term physiological parameter monitoring.

Since wearables are particularly helpful in monitoring chronic illnesses like heart failure or COPD, a long-term, autonomous use in an uncontrolled setting (like the patient's home) is envisaged. Ag/AgCl electrodes with conductive gel may present challenges for these applications: the patient's skin preparation may be difficult in an uncontrolled setting [46]; the conductive gel may be uncomfortable, raising the possibility of skin damage during extended measurements; and it may evaporate, degrading the quality of the signal [47]. For wearable devices, stiff electrodes composed of metallic plates are favoured over flexible electrodes that require conductive gel [46]. The adhesion problem during motion might be solved by flexible electrodes. Because of this, they are the most widely used kind, typically shown on a belt that is both elastic and adjustable [36,46–48]. A brief summary of the features of fabric-based flexible electrodes is as follows: the textile material used should have a high conductivity; cotton-based fabrics are better for increased comfort; the textile electrode should be a fixed component of the clothing for easier system application and stability; and the textile material should be easily cleaned and ironed [47]. The literature has widely suggested textile electrode belts with good performance [47, 48]. For brain EIT, Lin et al. also suggested dry and flexible electrodes [36]. In order to maintain low skin-electrode interface impedance even when moving, their method is based on a dry foam made of electrically conductive polymer foam coated in conductive fabric. This also permits a high degree of geometric conformity between the electrode and irregular scalp surface. These innovative electrode solutions

International Journal of Innovative Research in Science and Engineering
Volume 10, Issue 07, 2024
www.ijirse.com
ISSN: 2454-9665

generally outperform the conventional Ag/AgCl in terms of performance, but they are more wearable device friendly.

Table 2 provides a summary of the problems, difficulties, and creative solutions encountered during the electrode selection and design process.

Issue	Challenge	Innovative Solutions
Optimal number	Trade-off between image resolution and computation time	Rotational time
Correct positioning	Lack of robustness of image reconstruction algorithms	Elastic or adjustable electrode belt
Contact impedance	Modelling errors	Multi-pole measurement strategy; simultaneous reconstruction of electrodes and electrical properties; capacitively coupled EIT
Noise at the interface	Degradation of image resolution	Active electrode-based EIT
Ensure good contact	Variable contact impedance and reconstruction errors	Conductive gel; faulty contact detection algorithm
Ensure good contact (wearable systems)	Variable contact impedance and reconstruction errors	Dry and flexible electrodes

2.4. Design of Hardware

The block diagram of the hardware components is shown in Figure 1. The voltage-to-current converter, the DAC (which transforms the digital signal into an analogue signal), and the digital signal generator are all included in the current injection block. The data acquisition block, which houses the instrumentation amplifier, ADC, and demodulator, collects the voltage produced on the tissue's surface once the excitation current is delivered into it in accordance with the selected approach. The impedance distribution is recreated after processing the registered voltage's amplitude and phase.

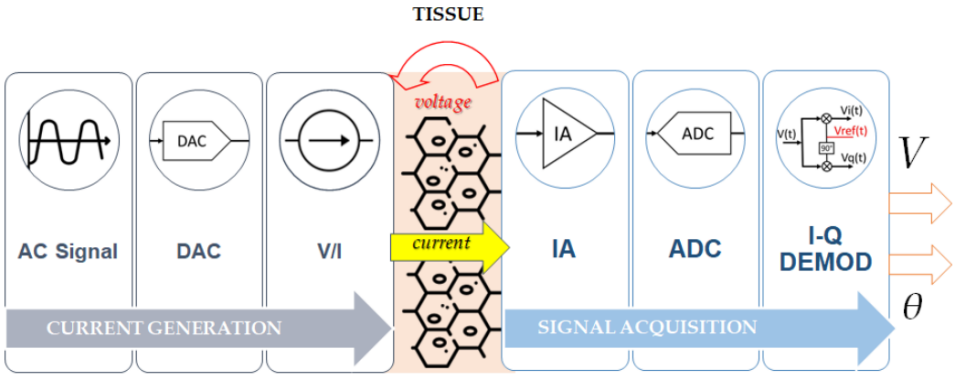

Current Level standards IEC 60601-1-2 4.1 (2023)

An illustration of an EIT signal acquisition platform's hardware components. The voltage-to-current (V/I) converter, the digital signal generator, and the digital to analogue converter (DAC) are components of the

ISSN: 2454-9665

current generation block. The tissue receives an injection of current, and the voltage Figure 1. Schematic schematic of an EIT signal acquisition platform's hardware components. The voltage-to-current (V/I) converter, the digital signal generator, and the digital to analogue converter (DAC) are components of the current generation block. After injecting the current into the tissue, the signal acquisition block—which houses the instrumentation amplifier (IA), the ADC, and the demodulator—acquires the voltage produced on the tissue's surface. The impedance distribution is recreated by processing the registered voltage's amplitude and phase.

2.4.1. Injection and Current Generation

A voltage-to-current converter or DAC-based open-drain current mirror can be used to achieve current injection [41]. A circuit known as a "current mirror" duplicates the current flowing through the input terminal onto the output terminal. The digital signal is converted into an analogue signal using a digital-to-analog converter (DAC), which is subsequently utilised to produce the excitation current. The voltage from the DAC amplifier is used as the input voltage by the voltage-to-current converter [27]. Square waves or pseudosine waves are the waveforms utilised to generate the signals [49]; the square wave has poor accuracy but good power efficiency, whereas Compared to a pure sine wave, the pseudo sine has less total harmonic distortion (THD) but more accuracy and power efficiency. While the pseudo sine wave has less total harmonic distortion (THD) than a pure sine wave, it nonetheless has good power efficiency and limited precision. The square wave has both power efficiency and accuracy. According to the IEC 60601-1-11:2015 standard [50], electrical safety considerations have the following limitations on the total input current level across all electrodes:

$$I = \begin{cases} 100\mu A_{rms} \; 0.1\ Hz < f < 1\ kHz \\ 100\mu A_{rms} \times \frac{f}{1\ kHz} \; 1\ kHz < f < 100\ kHz \\ 10\ mA_{rms} \; f > 100\ kHz \end{cases}$$

The current must be entirely differential for this application [51]; that is, the current at the current driver's source and the washbasin must be equal. The voltage that is measured in this scenario is the differential voltage that the current injection creates on the load. A common-mode voltage that results from a mismatch in current between the driver's source and sink can either saturate the current driver's output or produce a common-mode signal that the instrumentation amplifier has to reject in the voltage acquisition block's later stages [52]. A frequency-selective common mode feedback is provided in [53] in order to lower the common-mode voltage amplitude. By utilising an active feedback current sink in conjunction with a fully differential current driver that has a common mode rejection mechanism, the problem is lessened in [52].

Recent research suggests altering this fundamental arrangement to accomplish particular objectives. A buffer-mirrored current source is suggested in [54]; it guarantees a high SNR and a wide range of continuous current. In [55], an FPGA-generated input current is employed in a mirror circuit to create an adjustable current with varying frequencies and amplitudes. In [56], an FPGA is also utilised to carry out the acquisition for real-time imaging with a high sampling rate and accuracy. The digital signal in [27] is stored in the ROM by an FPGA and then transferred to the DAC at predetermined intervals to be converted into an analogue excitation voltage. A new current driver with a servo loop to modify the DC output voltage is introduced in [57].

2.4.2. Acquisition of Voltage Signals

In biomedical applications, the voltage signal acquisition circuit for EIT needs to have a high common-mode rejection ratio, a wide dynamic range, low noise, and high precision [58]. The presence of "U"-shaped voltages, which occur when the amplitude of the voltage signal obtained decreases with distance from the injecting electrodes and creates an odd pattern of voltage amplitude, allows the instrumentation amplifier to be connected with a programmable gain amplifier, or PGA [41]. A PGA can modify its gain by taking into account the significant variation in amplitude of each electrode pair's various measurements. Before the PGA [59], a pre-amplifier made up of a low-noise instrumentation amplifier is employed, potentially amplifying the input signal up to 514 times.

The automated gain controller (AGC) in [29] is connected to the PGA and dynamically modifies the PGA's gain according on the amplitude of the input. To capture signals across a wide dynamic range, this is essential.

In [60], the PGA is digitally controlled by the DSP and preceded by a unit gain amplifier to enhance the input impedance, with a maximum attainable gain of 8000 times the input signal. The acquisition system can take the boundary voltage into account to guarantee data accuracy.

The most used ADC type is the SAR ADC [61], which requires a sample rate in the mega samples per second range to meet the imaging system's frame rate requirements.

The most popular technique for demodulating bioimpedance measurements is called I-Q demodulation. Its goal is to extract the amplitude and phase of the acquired AC voltage signal by multiplying it by a reference signal to get the in-phase component and using a reference signal that has been shifted by 90 degrees to get the quadrature phase component [41].

In this scenario, we have an analogue matched filter. The in-phase and quadrature phase signals can be analogue signals that are filtered by the low-pass filter and transformed with an ADC. Alternatively, the digitalized original signal can be used to recover the in-phase and quadrature phase signals; in this scenario, a digital matching filter is available. Compared to an analogue filter with the same SNR, a digital filter uses less electricity [24].

Time stamp demodulation, pulse width demodulation, and magnitude and phase detection are the most often used demodulation techniques [41].

3. Application

A lot of factors, such as measurement noise, electrode count, current source, and voltage measuring methods, affect image resolution in the EIT hardware. For this reason, the image's spatial resolution differs among devices.

3.1. Pulmonary Imaging

Thoracic bioimpedance variation is primarily caused by two physiological processes: ventilation and perfusion. A bioimpedance change proportionate to the inspired gas volume is caused by the change in air volume during ventilation. Lung tissue impedance varies by around 5% during quiet breathing and up to 300% during heavy breathing [62]. Conversely, impedance changes of around 3% during systole and diastole are caused by pulmonary perfusion [63]. Real-time coverage of perfusion and breathing is possible with a temporal resolution

ISSN: 2454-9665

of 13 frames per second [64]. The images' spatial resolution is much poorer and restricted to the 2-3 cm gap between electrodes. A sample of around 5 cm of lung height is obtained using the traditional 16-electrode array arrangement.

Using existing imaging techniques [64–66] and additional reference methods, including spirometry [67,68], ventilation EIT imaging has been validated. Figure 2 reports representative EIT images illustrating the distribution of ventilation during silent breathing. The most promising use of ventilation EIT is mechanical ventilation monitoring, which eliminates the need to move patients and supportive equipment by providing real-time information on ventilation distribution at the bedside. Research has been done to monitor non-conventional mechanical ventilation modes [72] and to guide ventilator settings to reduce lung injury caused by ventilators [69–71]. Additionally, EIT can be utilised to spot unfavourable events that happen during mechanical breathing, like derecruitment or pneumothorax [73], allowing for early therapeutic intervention. EIT measures have been used to track therapies and interventions [75, 76], and studies have demonstrated that they are also possible in premature newborns [74, 75].

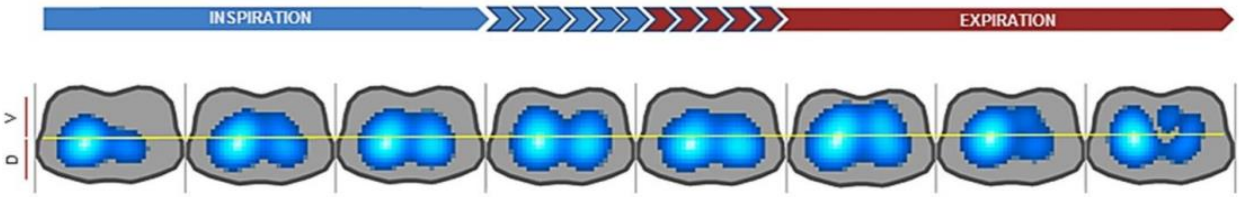

Figure 2. a series of electrical impedance tomography pictures that show how ventilation is distributed during silent breathing in the ventral (V) and dorsal (D) regions (Enlight 1800, Timpel SA, San Paulo, Brazil). The highest and lowest electrical impedance are represented by the gradation of colour from lighter to darker (greater and lower air displacement during the cycle). Courtesy of Armele Dornelas de Andrade and Caio CA Morais (Physiotherapy Department, Federal University of Pernambuco, Recife, Brazil)

The use of EIT to assess regional pulmonary perfusion has been the focus of recent studies. The main technique for determining perfusion by EIT is the measurement of impedance pulsatility during the cardiac cycle, which is based on electrocardiography gating or principal component analysis methods [77]. Another method is to inject an intravenous saline bolus and examine the tracer kinetics; this approach has only been published and validated in experimental experiments [78]. When calculating regional pulmonary perfusion, EIT perfusion imaging has shown a high degree of agreement with multidetector computer tomography (MDCT), the gold standard [78]. Many investigations using EIT imaging have been carried out in response to the recent outbreak of severe acute respiratory syndrome coronavirus-2 (SARS-CoV-2), demonstrating its potential to optimise therapeutic ventilation techniques [79,80].

Selecting suitable areas of interest (ROI) for the EIT scans is a major problem in the regional lung function imaging procedure. In order to achieve this goal, several approaches for lung area estimation have been investigated. These include active contouring techniques [82], ROI definition based on statistical techniques or geometrical considerations [81], principal component analysis [77], and functional tidal imaging.

3.2. Brain Imaging

Brain imaging uses the impedance variations in the cerebral cortex caused by a change in cerebral blood volume during functional activity or in cases of stroke and ischemia. This is because the blood has a lower impedance than the brain [83]. With current research concentrating on epilepsy, stroke, brain injury, and edoema, EIT offers a wide range of possibilities in diagnosis and real-time monitoring in patients with brain illnesses [83]. Research employing epicortical electrodes to examine conductivity alterations in the rat cerebral cortex during physiologically triggered activation [84] and epileptic discharges [84] has revealed temporal and spatial resolutions of 2 ms and 200 μm, for example. A penetration depth of 3 mm has been described for visualising epileptic activity in subcortical areas using epicortical electrodes [85]. An intriguing use case for the distinct real-time and portable features of EIT is the early and quick diagnosis of stroke, which is not possible with existing imaging methods. According to a recent study, cerebral ischemia in rats under anaesthesia causes an increase in impedance of roughly 60%, with an additional 10–20% identified at the cortical electrodes [86].

Capacitively coupled EIT (CCEIT) is being investigated as a potential replacement for the conventional EIT approach in brain imaging scenarios [40]. Using phantom, saline, and carrot samples, practical tests using a 12-electrode CCEIT device demonstrated the viability and potential of CCEIT for stroke imaging, identifying anomalies with a diameter of roughly 10 mm that were situated 30 mm from the boundary [40]. The viability of EIT has also been studied for real-time cerebral edoema monitoring [88] and for the detection of tiny brain haemorrhages (volumes of around 5 mL) [87, 88]. Because the skull is so resistant, brain imaging picture reconstruction is quite difficult. In certain cases, the image quality is also insufficient, such as when the distance between ischemia and bleeding is too tiny. One creative way to achieve more accurate, better contrast images is to use overlaid imagery for simultaneous reconstruction [89]. To do this, superimpose the reconstructed image of the secondary ischemia against the haemorrhage and the reconstructed image of the haemorrhage against the homogenous distribution [89].

While there are still a number of unresolved issues, EIT technology has the potential to be a valuable addition to traditional imaging techniques in the diagnosis and follow-up of cerebrovascular disease. It can facilitate the early identification of intracranial pathological alterations and offer practical instruments to enhance patient outcomes [83].

3.3. Thermoelectric Tracking

One effective and minimally invasive therapeutic option for solid tumours, including hepatocellular carcinoma, is hyperthermia [90]. Techniques used to treat solid tumours include microwave thermal ablation (MTA) and radiofrequency ablation (RFA). These methods are thought to have the potential to be beneficial because they are less intrusive and safer than alternative procedures. The underlying mechanism that results in cell death and intracellular protein denaturation [90, 91].

This therapeutic approach's basic working concept is the transformation of electromagnetic energy into heat, which results in the denaturation of intracellular proteins and the death of cells. In particular, the temperature is raised to 45–50 ◦C to cause cell disintegration, but it is kept safely away from temperatures beyond 90 ◦C that could have unfavourable effects such tissue carbonisation. This is why a cooling system is an essential

component of the RFA probe. Ensuring treatment specificity is a crucial prerequisite for these methods [90]. Therefore, methods that can precisely track the ablation's real-time evolution and the interior structures' temperature changes are required. The goal is to confirm that the ablation area completely encloses the tumour location and that no healthy tissue is left exposed [90,91]. Because temperature elevation affects tissue conductivity along the heated area and provides centimeter-scale spatial resolution, EIT is thought to be an appropriate approach for this purpose [90,91]. Furthermore, if the RFA probe is used as an additional electrode, the sensitivity is increased and a partially invasive form of EIT is produced [90].

EIT has been researched to track temperature variations during and after heating as well as during cooling [91]. Although phantoms and realistic human simulations were used in the investigations [90,91], in vivo tests are still required. To acquire precise estimations of the temperature in the living tissues that will be treated, it is also crucial to critically use a priori knowledge, such as data from literature surveys or data from other diagnostic procedures like MRIs [90].

While prevention of undesirable overheating and injury to healthy tissue is still being investigated, EIT was generally able to monitor the complete ablation of a tissue target [90]. Furthermore, future applications ought to concentrate on the effects of movement, electrical noise, and carbonisation above specific temperatures in order to enhance resolution and accuracy [90,91].

3.4. Tumor Detection

EIT may be able to detect tumours by taking advantage of the notable differences in conductivity and permittivity that many tumours have from the surrounding normal tissues [92–94]. In fact, more research is looking at the use of EIT for cancer screening and early detection; the primary use for this is for breast cancer, while it can also be used for skin, thyroid, liver, cervix, and lung cancer [92, 93, 95–102]. 3D maps of conductivity distributions in breast imaging have revealed detectable breast cancer models with sizes of around 12–14 mm [103], up to 5 mm with 4.9 m^{SM} sensitivity [104], using 3D systems with 128 and 90 electrodes, respectively. The CCERT (capacitively coupled electrical resistance tomography) technique is more appropriate for cancer detection than traditional EIT because it uses a higher frequency domain to obtain the relevant information for tumour detection, whereas EIT typically operates at frequencies lower than 1 MHz [95]. While EIT is a highly effective technique for dynamical imaging, time-difference imaging is less realistic in the context of tumour diagnosis since it is not realistic to get the patient's reference data prior to the tumor's development (i.e., baseline) [95]. In spite of this, phantom-based simulations and in vivo applications have demonstrated the effectiveness of EIT approaches in localising and differentiating lesions and diseased locations of cancer from normal tissues [92,93,95–102].

3.5. Assessment of Muscle Health

Electrical impedance myography is a non-invasive, painless technique that is used to evaluate the health of muscles; it could be replaced by EIT [105]. EIT has the potential to address several of the primary drawbacks of this method, including its reliance on the thickness of the skin and adipose tissue, its incapacity to identify closely spaced muscle groups, and its incapacity to evaluate the heterogeneity of muscle tissue. Additionally, studies have demonstrated that the combination of an ultrasound (US) equipment and an EIT system may yield

the most accurate and comprehensive data while also improving image quality. Through the detection of changes in the electrical properties of muscles, studies carried out on phantoms, simulation systems, and patients have demonstrated the effectiveness of the combined US/EIT system in capturing various healthy and pathological muscle features. More specifically, EIT is a promising tool for non-invasive and spatially localised assessment of muscle health because US/EIT systems can distinguish between physiological and pathological conditions by detecting differences in muscle (longitudinal and transverse) conductivity and permittivity [105].

4. Wearable Solutions

4.1. Hardware Characteristics

A wearable device [106] is a system that is integrated into clothing or worn on the human body. It is primarily made up of receptors, including electrodes or microminiaturized sensors, that can detect and transfer the collected data to a processing unit using common communication protocols. On a PC or smartphone, the gathered signals can be extended to extract valuable information with the help of specialised software and algorithms. The majority of portable EIT systems, which typically consist of a belt or wrist wrap with embedded electrodes, are designed to be used for daily non-invasive monitoring in both clinics and at home. The purpose of portable EIT devices is to monitor alterations in bodily fluid and pulmonary gas to track physiological changes in the body.

Initially, researchers concentrated mostly on the wireless data transfer and microminiaturization of the traditional EIT system [107], attempting to address the problem of bulky volume. Their module also has the ability to digitally process the obtained signals on a separate FPGA and pre-filter them.

4.1.1. Low Power Consumption

Because portable energy sources, such as batteries, have limited power availability and a tendency to degrade over time, it is necessary to achieve low power consumption for portable applications. In order to maximise the current flowing in the load, a high output impedance must then be achieved in the current driver stage [56]. There are two types of current generators: oscillator-based and DAC-based. For portable devices, the latter is preferred due to its reduced power consumption [49]. Lower frequencies can be processed at a lower sample rate when it comes to the ADC in order to prevent oversampling and reduced power consumption in the ADC SAR [61]. At the demodulation step, a few particular adjustments have also been made. In the demodulation step, several particular adjustments have also been made. I-Q demodulation is shown in [46,104]. Although the input referred noise is larger, this approach is efficient in terms of power consumption since it operates the signal processing chain's later steps at lower frequencies and eliminates the need for extra low pass filters. Fast I-Q demodulation is used in the cited works to minimise power consumption. For signals at 10 kHz, this reduces the settling time, enabling a real-time operation of 5 frames per second.

4.1.2. Electrode Configuration

As mentioned in Section 2.3.6 above, selecting the right electrodes is a crucial aspect of wearable device design. The primary sources of limitation are the variations between operators in how the electrodes are used, which necessitates their viability in both home and clinical settings; prolonged use, which dries out the conductive gel required for Ag/AgCl electrodes; and, primarily, use while moving, which introduces artefacts. Applying a belt

ISSN: 2454-9665

of dry electrodes composed of conductive fabric is the most widely utilised solution. It has been demonstrated through experiments that there are no variations when compared to Ag/AgCl electrode measurements [48]. However, there is a greater chance of displacement with dry electrodes, which could result in motion artefacts. Utilising a wearable wireless belt with dry electrodes in conjunction with the Gauss-Newton method to optimise the EIT image is an intriguing idea [36]. This study highlights that using dry electrodes can result in better durability and increased comfort due to a decreased risk of skin irritation. Furthermore, the results showed that the reconstruction algorithm accurately located the objects in the images, and that in a human experiment, the variations in the ratios of the lung area to the whole chest during inhalation and exhalation matched the physiological changes of typical lung activity. As previously indicated, studies based on the integration of textile electrodes with a garment belt have been published.

Wearable systems may demand more strict qualities in terms of noise and the input dynamic range of the electrodes due to reduced signal amplitudes, in addition to the fundamental requirements for the voltage acquisition circuits in classic EIT [49].

4.1.3. Examples of Wearable EIT Implementations

In this paper, two exemplary hardware solutions from investigations on human lung ventilation are reported as examples. The first study [48] focuses on a belt with 16 embossed nanofiber web electrodes comprised of metallic threads and Ag-plated PVDF nanofiber web that are intended to make good skin contact. With a broad contact area and padding behind each electrode, it achieves better comfort and lower contact impedance; contact impedance and stability were found to be similar to Ag/AgCl electrodes. The belt is made to fit a variety of thorax sizes because it has an adjustable inner band. Additionally, sponges have been inserted into pockets on the outer band to provide tight contact with the body in order to better conform the shape to the chest. Finally, the EIT acquisition system uses a conventional ECG electrode as a reference. The performance of belt-mounted electrodes has been proven to be more stable over time than adhesive electrodes, even if the proposed electrodes permit higher resting noise levels.

In the second piece of art [47], a belt with sixteen textile electrodes—silver wire cloth on the outside and cotton on the inside—is featured. The suggested device's validity was demonstrated by experimental results that were in line with those obtained from commercial ECG electrodes. It was also discovered that the impedance fields were larger, which improved image discrimination.

A system built on a novel cooperative sensor solution serves as an example of how other proposed solutions can acquire signals simultaneously [108]. A sensor architecture for simultaneous ECG data capture and frequency-multiplexed EIT is presented in this work. This topology has the advantages of adjustable EIT stimulation and measurement patterns and a large reduction in cabling complexity. Cooperative sensors, which only come into touch with the skin, digitally transfer data between the master device and the sensors over a bidirectional communication channel. The 16 sensors in the proposed system are spaced equally across the transverse plane and connected to the elastic belt. Four sensors are additionally positioned in the infraclavicular regions for the purpose of acquiring ECG data. The master device is situated above the belt on the right ventral portion of the thorax. The primary benefit of this gadget is that it offers continuous measurement because the sensors sense

ISSN: 2454-9665

skin contact and activate automatically until the patient removes the vest. At the conclusion of the acquisition session, data are saved in the master device and wirelessly transferred to a computer.

4.2. Applications of Wearable EIT

Many sectors, including pulmonary imaging, cancer detection, and gesture recognition, have suggested wearable EIT devices. Moreover, multiparametric monitoring has been achieved by integrating these sensors with other measuring systems in the past.

4.2.1. Pulmonary Imaging

The most common use of wearable technology is in pulmonary imaging. Since the electrical characteristics of healthy and edematous lung tissue fluctuate due to changes in the mix of liquid and air, monitoring lung resistivity has been proposed as a means of detecting pulmonary edoema [109]. These devices integrate the transthoracic and EIT techniques to provide a low-cost, long-term, continuous, and safe system that doesn't require ionising radiation. The ECG signal and the left and right lung resistivity values are important for coordinating the procedure.

Unfortunately, there are still certain drawbacks. The former method relies heavily on anthropometric factors and is unable to detect the impedance of internal organs directly, whilst the latter requires a large number of electrodes and is extremely susceptible to measurement noise. A device with 32 active electrodes and an application-specific integrated circuit (ASIC) installed on a flexible printed circuit board wrapped inside the belt was proposed by another study [42] for cardio-pulmonary monitoring. This wearable system is among the quickest due to its unique feature of using two parallel EIT data collecting channels to produce a frame rate of 107 fps. In order to help with the selection of the EIT model, the device can also capture additional information, such as heart rate, ambient temperature and humidity, and the shape and position of the thorax.

4.2.2. Cancer Detection

For the purpose of early breast cancer diagnosis, a high-resolution EIT integrated circuit has been proposed. A portable EIT device that can identify a 5 mm cancer mass has been put together by researchers and shaped like a brassier [29]. A multi-layered fabric circuit board with two reference electrodes for voltage detection and current stimulation and 90 electrodes organised in five concentric rings has been used to integrate the circuit. Researchers ran simulations to find the bare minimum of sensors needed for good sensitivity, and the result was eighty. The finished product is small, extremely sensitive, and has a mobile smart device connection for early breast cancer diagnosis.

4.2.3. Gesture Recognition

The EIT device is used to monitor the inner conductivity distributions induced by forearm bone and muscle movement in a well researched application called gesture recognition. The system is able to recognise 19 hand gestures with an accuracy of 98% using the round-robin sub-grouping method. An example has been proposed in [110], which presents a wearable device composed of a wrist wrap with embedded electrodes. The data is passed to a deep learning neural network for gesture recognition. The method could be optimised by reducing the number of robins while keeping a high classification accuracy. A new publication [111] presents an additional instance that utilises machine learning methods and the two-terminal EIT methodology. The device

operates at a pace of eight frames per second and recognises nine distinct gestures. Because it uses a quadratic discriminant algorithm as its classification model, it uses fewer electrodes than earlier efforts and achieves an accuracy gain of approximately 98.5%.

These EIT devices should not be utilised with other bioimpedance measurement methods in order to preserve data quality because the injected high frequency currents may affect the signals. Subsequent research endeavours will involve refining the suggested systems through enhanced spatial resolution. Additionally, more research needs to be done to determine whether it is feasible to monitor people using portable devices.

4.2.4. Multi-Parameter EIT

Finally, the development of a belt for thorax vital multiple sign monitoring has been the main focus of wearable EIT solutions. It has been suggested to use a system with 16 active electrodes, each of which is linked to an ASIC [44]. This system enables voltage-sensing patterns and programmable, adaptable electrode current driving under straightforward digital control. The gadget can record breathing cycle, heart rate, and boundary shape information in addition to high-quality lung ventilation images at a frame rate of 122 fps. The high-performance ASIC, which offers an improved common-mode rejection ratio while simplifying the wiring and digital control, is the novel feature presented in this work. A few years prior [43], a comparable solution was unveiled. It consists of an active electrode integrated circuit composed of two shape sensor buffers, a low noise voltage amplifier, and a wideband high-power current driver. With tools that can generate a continuous tidal volume signal from real-time EIT lung ventilation images, the diagnosis of sleep apnea and hypoventilation to complement polysomnography and home sleep studies has also been studied [112].

4.3. Integration in Telemedicine Platforms

As previously indicated, certain wearable EIT devices currently come with corresponding smartphone applications that provide portable access to the results. Wearable EIT can often be included into telemedicine platforms by being integrated into body area networks (BANs). In particular, body area networks, or BANs for short, are made up of a network of wearable devices that can be inserted into the body, fastened to the body, or carried by the user in a bag, pocket, or on their hand [113]. The second group includes wearable EIT devices, which are affixed to the body in certain positions.

In addition to the wearable EIT device, other sensors have also been cited in a number of situations. Because it is so simple to position in a belt, an ECG device was frequently mentioned as a component of the system in the wearable EIT segment. A sensor system that may give many signal kinds, including bio-impedance, electrical biopotentials like ECG and EMG, and temperature and humidity signals, has been installed in some devices [46]. One of these devices is a belt that has sixteen electrodes (current and potential electrodes) placed in it that can measure ECG and EIT signals. One of these devices is a belt that has sixteen electrodes (current and potential electrodes) placed in it that can measure ECG and EIT signals. A wearable EIT device, an ECG, a three-axial accelerometer to measure body movement, and a pulse oximeter to determine peripheral blood oxygen saturation can all be simultaneously acquired by other suggested systems [108]. In order to estimate continuous tidal volume, a wearable system was proposed in the study [112]. It consists of a chest belt (16 electrodes for EIT imaging and ECG data acquisition), a finger sensor, a microphone to record snoring sounds,

an accelerometer, a gyroscope, and a magnetometer to detect body position. The multi-parameter module, which is controlled by an FPGA, is located in the middle of the chest and contains the necessary sensors and circuits.

The design of most telemedicine platforms is two hops; Figure 3 illustrates this with an EIT device. Sensor data is sent by sensor-manager link technologies to a gateway, which subsequently sends the data to the data management section using cellular technology.

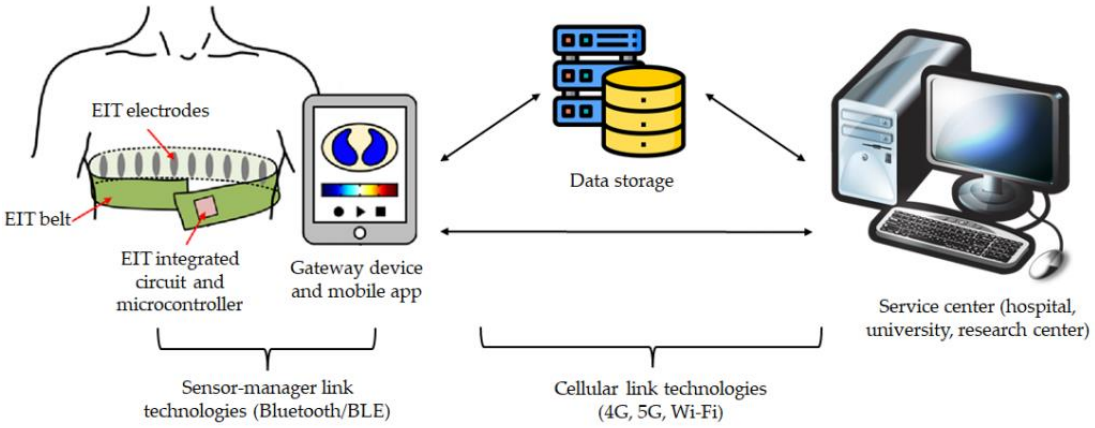

Figure 3: Two-hop architectural telemedicine system with EIT device; taken from [115,116]. The microcontroller and additional parts, together with the EIT electrodes, are mounted on a belt. Sensor-manager link technologies, like Bluetooth, are used to transmit data to a gateway device, which is typically a tablet or smartphone. On the gateway device, a mobile app for real-time picture visualisation can be installed. A distant service centre can retrieve the outcomes of data sent by the gateway device via cellular link technologies to a central database (data storage).

In other situations, such as one of the previously stated research [108], the signal-acquiring devices are connected to the internet using cellular connection technologies, such as wi-fi, thus there is no sensor-manager link technology. This is frequently the case when wearing sensor-containing clothing [115], since sensors can be wired to a master data logger. As previously mentioned, wearable EIT devices can be thought of as smart clothing and could offer many indications of interest at once.

5. Discussion

The evolution of EIT hardware design and applications—from traditional to wearable solutions—has been the main topic of this review. EIT as a medical imaging technique has shown certain unusual characteristics. It has a high temporal resolution, is non-invasive, and doesn't require ionising radiation. Furthermore, the equipment's low cost and superior portability make it appropriate for both long-term and real-time bedside monitoring, for example, in the case of patients—like ICU patients—who are difficult to move to other areas of the hospital. The primary drawbacks are the reduced spatial resolution in comparison to alternative imaging modalities, the reduced susceptibility to relevant phenomena, and the elevated susceptibility to flaws in the hardware and electrode-body interface. Nevertheless, a growing body of research focusing on refining reconstruction algorithms and optimising measurement configurations has been conducted in tandem with the growing

scientific interest in EIT [117]. Furthermore, the COVID-19 pandemic has served as the ideal setting for the use of EIT, advancing both its technological advancement and use.

EIT systems have shifted towards wearable solutions, which have more portability, less power consumption, and application-specific design—as covered in depth in Section 4. EIT systems are less cumbersome thanks to the wearable approach, which enables the use of a wireless EIT module with a tiny volume [107]. With a few modifications, EIT electrodes in wearable devices can be incorporated into clothing and used in motion with satisfactory outcomes.

The potential for wearable and wireless EIT devices opens up new applications for these systems, like patient monitoring from a distance even during ordinary life. Moreover, wearable EIT devices can be requested in addition to other diagnostic methods in the event that abnormalities are found through ongoing EIT monitoring, effectively serving as a "early-warning system" with EIT technology.

6. Conclusions

A current or voltage pattern is injected through electrodes placed on the patient's skin as part of the EIT medical imaging technology, which then reconstructs the interior conductivity distribution using the voltages the electrodes have collected. When compared to alternative imaging methods, EIT offers significant benefits. In actuality, EIT is non-invasive, produces no ionising radiation, and has a high temporal resolution. Furthermore, its excellent portability and inexpensive cost make it appropriate for bedside monitoring in real time. EIT can be used as an extra tool when other medical imaging techniques aren't working, but it can't replace them due to its low spatial resolution.

The potential to use EIT in the creation of wearable gadgets has recently given this technology a push. This study reviews the existing research on EIT systems, including everything from clinical applications to hardware design. The creation of wearable and wireless EIT technology may strengthen the method's application in clinical settings and expand its range of scenarios, such as remote monitoring in uncontrolled settings like patient homes.

References

[1]. Bayford, R.; Tizzard, A. Bioimpedance Imaging: An Overview of Potential Clinical Applications. Analyst 2012, 137, 4635–4643. [CrossRef] [PubMed]

[2]. Rafiei-Naeini, M.; McCann, H. Low-Noise Current Excitation Sub-System for Medical EIT. Physiol. Meas. 2008, 29, S173. [CrossRef] [PubMed]

[3]. Sadleir, R.J.; Fox, R.A.; Turner, V.F. Inflatable belt for the application of electrode arrays. Rev. Sci. Instrum. 2000, 71, 530–535. [CrossRef]

[4]. Dong, G.; Bayford, R.; Liu, H.; Zhou, Y.; Yan, W. EIT Images with Improved Spatial Resolution Using a Realistic Head Model. In Proceedings of the Annual International Conference of the IEEE Engineering in Medicine and Biology Society, New York, NY, USA, 30 August–3 September 2006; Volume 2006, pp. 1134–1137.

[5]. Liu, S.; Jia, J.; Zhang, Y.D.; Yang, Y. Image Reconstruction in Electrical Impedance Tomography Based on Structure-Aware Sparse Bayesian Learning. IEEE Trans. Med. Imaging 2018, 37, 2090–2102. [CrossRef]

[6]. Brown, B.H. Electrical Impedance Tomography (EIT): A Review. J. Med. Eng. Technol. 2003, 27, 97–108. [CrossRef]

[7]. Lionheart, W.R.B. EIT Reconstruction Algorithms: Pitfalls, Challenges and Recent Developments. Physiol. Meas. 2004, 25, 125–142. [CrossRef]

[8]. Dijkstra, A.M.; Brown, B.H.; Leathard, A.D.; Harris, N.D.; Barber, D.C.; Edbrooke, D.L. Review Clinical Applications of Electrical Impedance Tomography. J. Med. Eng. Technol. 1993, 17, 89–98. [CrossRef]

[9]. Khalil, S.F.; Mohktar, M.S.; Ibrahim, F. The Theory and Fundamentals of Bioimpedance Analysis in Clinical Status Monitoring and Diagnosis of Diseases. Sensors 2014, 14, 10895–10928. [CrossRef]

[10]. Gabriel, S.; Lau, R.W.; Gabriel, C. The Dielectric Properties of Biological Tissues: III. Parametric Models for the Dielectric Spectrum of Tissues. Phys. Med. Biol. 1996, 41, 2271–2293. [CrossRef]

[11]. Nopp, P.; Rapp, E.; Pfutzner, H.; Nakesch, H.; Rusham, C. Dielectric Properties of Lung Tissue as a Function of Air Content. Phys. Med. Biol. 1993, 38, 699–716. [CrossRef]

[12]. Schwan, H.P. Electrical Properties of Tissue and Cell Suspensions. Adv. Biol. Med. Phys. 1957, 5, 147–209. [CrossRef] [PubMed]

[13]. Gabriel, C.; Gabriel, S.; Corthout, E. The Dielectric Properties of Biological Tissues: I. Literature Survey. Phys. Med. Biol. 1996, 41, 2231–2249. [CrossRef] [PubMed]

[14]. Kyle, U.G.; Bosaeus, I.; De Lorenzo, A.D.; Deurenberg, P.; Elia, M.; Gómez, J.M.; Heitmann, B.L.; Kent-Smith, L.; Melchior, J.C.; Pirlich, M.; et al. Bioelectrical Impedance Analysis—Part I: Review of Principles and Methods. Clin. Nutr. 2004, 23, 1226–1243. [CrossRef] [PubMed]

[15]. Packham, B.; Koo, H.; Romsauerova, A.; Ahn, S.; McEwan, A.; Jun, S.C.; Holder, D.S. Comparison of Frequency Difference Reconstruction Algorithms for the Detection of Acute Stroke Using EIT in a Realistic Head-Shaped Tank. Physiol. Meas. 2012, 33. 767–786. [CrossRef]

[16]. Lee, J.M.; Uhlmann, G. Determining Anisotropic Real-analytic Conductivities by Boundary Measurements. Commun. Pure Appl. Math. 1989, 42, 1097–1112. [CrossRef]

[17]. Khan, T.A.; Ling, S.H. Review on Electrical Impedance Tomography: Artificial Intelligence Methods and Its Applications. Algorithms 2019, 12, 88. [CrossRef]

[18]. Brazey, B.; Haddab, Y.; Zemiti, N. Robust Imaging Using Electrical Impedance Tomography: Review of Current Tools. Proc. R. Soc. A Math. Phys. Eng. Sci. 2022, 478, 20210713. [CrossRef]

[19]. Riera, J.; Riu, P.J.; Casan, P.; Masclans, J.R. Tomografía de Impedancia Eléctrica En La Lesión Pulmonar Aguda. Med. Intensiv. 2011, 35, 509–517. [CrossRef]

[20]. Nissinen, A.; Kolehmainen, V.P.; Kaipio, J.P. Compensation of Modelling Errors Due to Unknown Domain Boundary in Electrical Impedance Tomography. IEEE Trans. Med. Imaging 2011, 30, 231–242. [CrossRef]

[21]. Adler, A.; Holder, D. Electrical Impedance Tomography: Methods, History and Applications; CRC Press: Boca Raton, FL, USA, 2021, ISBN 9780429399886.

ISSN: 2454-9665

[22]. Seo, J.K.; Harrach, B.; Woo, E.J. Recent Progress on Frequency Difference Electrical Impedance Tomography. ESAIM Proc. 2009, 26, 150–161. [CrossRef]

[23]. Wu, C.; Soleimani, M. Frequency Difference EIT with Localization: A Potential Medical Imaging Tool during Cancer Treatment. IEEE Access 2019, 7, 21870–21878. [CrossRef]

[24]. Takhti, M.; Odame, K. Structured Design Methodology to Achieve a High SNR Electrical Impedance Tomography. IEEE Trans. Biomed. Circuits Syst. 2019, 13, 364–375. [CrossRef] [PubMed] Anand, S.; Jandial, P.; Nersisson, R. A Technical Survey on Hardware Configurations for Electrical Impedance Tomography Systems. In Proceedings of the 3rd IEEE International Virtual Conference on Innovations in Power and Advanced Computing Technologies, i-PACT 2021, Kuala Lumpur, Malaysia, 27–29 November 2021.

[25]. Harikumar, R.; Prabu, R.; Raghavan, S. Electrical Impedance Tomography (EIT) and Its Medical Applications: A Review. Int. J. Soft Comput. Eng. 2013, 3, 193–198.

[26]. Rosa, B.M.G.; Yang, G.Z. Bladder Volume Monitoring Using Electrical Impedance Tomography with Simultaneous Multi-Tone Tissue Stimulation and DFT-Based Impedance Calculation Inside an FPGA. IEEE Trans. Biomed. Circuits Syst. 2020, 14, 775–786. [CrossRef]

[27]. Halter, R.J.; Hartov, A.; Paulsen, K.D. A Broadband High-Frequency Electrical Impedance Tomography System for Breast Imaging. IEEE Trans. Biomed. Eng. 2008, 55, 650–659. [CrossRef]

[28]. Hong, S.; Lee, K.; Ha, U.; Kim, H.; Lee, Y.; Kim, Y.; Yoo, H.J. A 4.9 MΩ-Sensitivity Mobile Electrical Impedance Tomography IC for Early Breast-Cancer Detection System. IEEE J. Solid-State Circuits 2015, 50, 245–257. [CrossRef]

[29]. Kim, M.; Jang, J.; Kim, H.; Lee, J.; Lee, J.; Lee, J.; Lee, K.R.; Kim, K.; Lee, Y.; Lee, K.J.; et al. A 1.4-m Ω-Sensitivity 94-DB Dynamic-Range Electrical Impedance Tomography SoC and 48-Channel Hub-SoC for 3-D Lung Ventilation Monitoring System. IEEE J. Solid-State Circuits 2017, 52, 2829–2842. [CrossRef]

[30]. Xu, G.; Wang, R.; Zhang, S.; Yang, S.; Justin, G.A.; Sun, M.; Yan, W. A 128-Electrode Three Dimensional Electrical Impedance Tomography System. In Proceedings of the Annual International Conference of the IEEE Engineering in Medicine and Biology, Lyon, France, 22–26 August 2007; Volume 2007, pp. 4386–4389.

[31]. Huang, C.N.; Yu, F.M.; Chung, H.Y. Rotational Electrical Impedance Tomography. Meas. Sci. Technol. 2007, 18, 2958–2966. [CrossRef]

[32]. Lehti-Polojarvi, M.; Koskela, O.; Seppanen, A.; Figueiras, E.; Hyttinen, J. Rotational Electrical Impedance Tomography Using Electrodes with Limited Surface Coverage Provides Window for Multimodal Sensing. Meas. Sci. Technol. 2018, 29, 025401. [CrossRef]

[33]. Murphy, E.K.; Mahara, A.; Halter, R.J. Absolute Reconstructions Using Rotational Electrical Impedance Tomography for Breast Cancer Imaging. IEEE Trans. Med. Imaging 2017, 36, 892–903. [CrossRef]

[34]. Gaggero, P.O.; Adler, A.; Brunner, J.; Seitz, P. Electrical Impedance Tomography System Based on Active Electrodes. Physiol. Meas. 2012, 33, 831–847. [CrossRef]

[35]. Lin, B.S.; Yu, H.R.; Kuo, Y.T.; Liu, Y.W.; Chen, H.Y.; Lin, B.S. Wearable Electrical Impedance Tomography Belt With Dry Electrodes. IEEE Trans. Biomed. Eng. 2022, 69, 955–962. [CrossRef] [PubMed]

[36]. Boone, K.G.; Holder, D.S. Effect of Skin Impedance on Image Quality and Variability in Electrical Impedance Tomography: A Model Study. Med. Biol. Eng. Comput. 1996, 34, 351–354. [CrossRef] [PubMed]

[37]. Hua, P.; Woo, E.J.; Webster, J.G.; Tompkins, W.J. Using Compound Electrodes In Electrical Impedance Tomography. IEEE Trans. Biomed. Eng. 1993, 40, 29–34. [CrossRef] [PubMed]

[38]. Agnelli, J.P.; Kolehmainen, V.; Lassas, M.J.; Ola, P.; Siltanen, S. Simultaneous Reconstruction of Conductivity, Boundary Shape, and Contact Impedances in Electrical Impedance Tomography. SIAM J. Imaging Sci. 2021, 14, 1407–1438. [CrossRef]

[39]. Jiang, Y.D.; Soleimani, M. Capacitively Coupled Electrical Impedance Tomography for Brain Imaging. IEEE Trans. Med. Imaging 2019, 38, 2104–2113. [CrossRef]

[40]. Wu, Y.; Hanzaee, F.F.; Jiang, D.; Bayford, R.H.; Demosthenous, A. Electrical Impedance Tomography for Biomedical Applications: Circuits and Systems Review. IEEE Open J. Circuits Syst. 2021, 2, 380–397. [CrossRef]

[41]. Wu, Y.; Jiang, D.; Bardill, A.; De Gelidi, S.; Bayford, R.; Demosthenous, A. A High Frame Rate Wearable EIT System Using Active

[42]. Electrode ASICs for Lung Respiration and Heart Rate Monitoring. IEEE Trans. Circuits Syst. I Regul. Pap. 2018, 65, 3810–3820. [CrossRef]

[43]. Wu, Y.; Langlois, P.; Bayford, R.; Demosthenous, A. Design of a CMOS Active Electrode IC for Wearable Electrical Impedance Tomography Systems. In Proceedings of the IEEE International Symposium on Circuits and Systems, Montreal, QC, Canada, 22–25 May 2016; Volume 2016, pp. 846–849.

[44]. Wu, Y.; Jiang, D.; Bardill, A.; Bayford, R.; Demosthenous, A. A 122 Fps, 1 MHz Bandwidth Multi-Frequency Wearable EIT Belt Featuring Novel Active Electrode Architecture for Neonatal Thorax Vital Sign Monitoring. IEEE Trans. Biomed. Circuits Syst. 2019, 13, 927–937. [CrossRef]

[45]. Asfaw, Y.; Adler, A. Automatic Detection of Detached and Erroneous Electrodes in Electrical Impedance Tomography. Physiol. Meas. 2005, 26, S175. [CrossRef]

[46]. Rymarczyk, T.; Nita, P.; Vejar, A.; Wos, M.; Oleszek, M.; Adamkiewicz, P. Architecture of a Mobile System for the Analysis of Biomedical Signals Based on Electrical Tomography. In Proceedings of the 2018 Applications of Electromagnetics in Modern Techniques and Medicine, PTZE 2018, Raclawice, Poland, 9–12 September 2018; pp. 289–292.

[47]. Hu, C.L.; Cheng, I.C.; Huang, C.H.; Liao, Y.T.; Lin, W.C.; Tsai, K.J.; Chi, C.H.; Chen, C.W.; Wu, C.H.; Lin, I.T.; et al. Dry Wearable Textile Electrodes for Portable Electrical Impedance Tomography. Sensors 2021, 21, 6789. [CrossRef] [PubMed]

[48]. Oh, T.I.; Kim, T.E.; Yoon, S.; Kim, K.J.; Woo, E.J.; Sadleir, R.J. Flexible Electrode Belt for EIT Using Nanofiber Web Dry Electrodes. Physiol. Meas. 2012, 33, 1603–1616. [CrossRef] [PubMed]

[49]. Van Helleputte, N.; Konijnenburg, M.; Pettine, J.; Jee, D.W.; Kim, H.; Morgado, A.; Van Wegberg, R.; Torfs, T.; Mohan, R.; Breeschoten, A.; et al. A 345 Mw Multi-Sensor Biomedical SoC with Bio-Impedance, 3-Channel ECG, Motion Artifact Reduction, and Integrated DSP. IEEE J. Solid-State Circuits 2015, 50, 230–244. [CrossRef]

[50]. IEC 60601-1:2015; Medical Electrical Equipment Part 1: General Requirements for Basic Safety and Essential Performance. ISO: Geneva, Switzerland, 2015.

[51]. Zeng, L.; Heng, C.H. An 8-Channel 1.76-MW 4.84-Mm2Electrical Impedance Tomography SoC with Direct If Frequency Division Multiplexing. IEEE Trans. Circuits Syst. II Express Briefs 2021, 68, 3401–3405. [CrossRef]

[52]. Wu, Y.; Jiang, D.; Langlois, P.; Bayford, R.; Demosthenous, A. A CMOS Current Driver with Built-in Common-Mode Signal Reduction Capability for EIT. In Proceedings of the ESSCIRC 201743rd IEEE European Solid State Circuits Conference, Leuven, Belgium, 11–14 September 2017; pp. 227–230.

[53]. Langlois, P.J.; Wu, Y.; Bayford, R.H.; Demosthenous, A. On the Application of Frequency Selective Common Mode Feedback for Multifrequency EIT. Physiol. Meas. 2015, 36, 1337–1350. [CrossRef]

[54]. Wicaksono, R.; Baidillah, M.R.; Darma, P.N.; Inoue, A.; Tsuji, H.; Takei, M. Pocket Electrical Impedance Tomography (p-EIT) System with Wide Impedance Range Buffer- Mirrored Current Source (BMCS) with Assist of Filter-Trained Quasi-3-D Method for Functional Gastric-Shape Imaging. IEEE Trans. Instrum. Meas. 2021, 70, 4507317. [CrossRef]

[55]. Xu, Y.; Yan, Z.; Han, B.; Dong, F. An FPGA-Based Multifrequency EIT System with Reference Signal Measurement. IEEE Trans. Instrum. Meas. 2021, 70, 4500710. [CrossRef]

[56]. Li, W.; Xia, J.; Zhang, G.; Ma, H.; Liu, B.; Yang, L.; Zhou, Y.; Dong, X.; Fu, F.; Shi, X. Fast High-Precision Electrical Impedance Tomography System for Real-Time Perfusion Imaging. IEEE Access 2019, 7, 61570–61580. [CrossRef]

[57]. Shahghasemi, M.; Odame, K.M. A Wide-Band, Wide-Swing Current Driver for Electrical Impedance Tomography Applications. In Proceedings of the Midwest Symposium on Circuits and Systems, Springfield, MA, USA, 9–12 August 2020; Volume 2020, pp. 659–662.

[58]. Shi, X.; Li, W.; You, F.; Huo, X.; Xu, C.; Ji, Z.; Liu, R.; Liu, B.; Li, Y.; Fu, F.; et al. High-Precision Electrical Impedance Tomography Data Acquisition System for Brain Imaging. IEEE Sens. J. 2018, 18, 5974–5984. [CrossRef]

[59]. Shi, X.; You, F.; Xu, C.; Ji, Z.; Liu, R.; Dong, X.; Fu, F.; Huo, X. Design and Implementation of a High-Precision Electrical Impedance Tomography Data Acquisition System for Brain Imaging. In Proceedings of the 2016 IEEE Biomedical Circuits and Systems Conference, BioCAS 2016, Shanghai, China, 17–19 October 2016; pp. 9–13.

[60]. Yang, D.; Huang, G.; Xu, B.; Wang, X.; Wang, Z.; Wei, Z. A DSP-Based EIT System with Adaptive Boundary Voltage Acquisition. IEEE Sens. J. 2022, 22, 5743–5754. [CrossRef]

[61]. Takhti, M.; Teng, Y.C.; Odame, K. A 10 MHz Read-Out Chain for Electrical Impedance Tomography. IEEE Trans. Biomed. Circuits Syst. 2018, 12, 222–230. [CrossRef] [PubMed]

[62]. Tomicic, V.; Cornejo, R. Lung Monitoring with Electrical Impedance Tomography: Technical Considerations and Clinical Applications. J. Thorac. Dis. 2019, 11, 3122–3135. [CrossRef] [PubMed]

[63]. Visser, K.R. Electric Properties of Flowing Blood and Impedance Cardiography. Ann. Biomed. Eng. 1989, 17, 463–473. [CrossRef] [PubMed]

[64]. Wrigge, H.; Zinserling, J.; Muders, T.; Varelmann, D.; Günther, U.; Von Der Groeben, C.; Magnusson, A.; Hedenstierna, G.; Putensen, C. Electrical Impedance Tomography Compared with Thoracic Computed Tomography during a Slow Inflation Maneuver in Experimental Models of Lung Injury. Crit. Care Med. 2008, 36, 903–909. [CrossRef] [PubMed]

[65]. Frerichs, I.; Hinz, J.; Herrmann, P.; Weisser, G.; Hahn, G.; Dudykevych, T.; Quintel, M.; Hellige, G. Detection of Local Lung Air Content by Electrical Impedance Tomography Compared with Electron Beam CT. J. Appl. Physiol. 2002, 93, 660–666. [CrossRef] [PubMed]

[66]. Richard, J.C.; Pouzot, C.; Gros, A.; Tourevieille, C.; Lebars, D.; Lavenne, F.; Frerichs, I.; Guérin, C. Electrical Impedance Tomography Compared to Positron Emission Tomography for the Measurement of Regional Lung Ventilation: An Experimental Study. Crit. Care 2009, 13, R82. [CrossRef]

[67]. Hinz, J.; Moerer, O.; Neumann, P.; Dudykevych, T.; Hellige, G.; Quintel, M. Effect of Positive End-Expiratory-Pressure on Regional Ventilation in Patients with Acute Lung Injury Evaluated by Electrical Impedance Tomography. Eur. J. Anaesthesiol. 2005, 22, 817–825. [CrossRef]

[68]. Coulombe, N.; Gagnon, H.; Marquis, F.; Skrobik, Y.; Guardo, R. A Parametric Model of the Relationship between EIT and Total Lung Volume. Physiol. Meas. 2005, 26, 401–411. [CrossRef]

[69]. Meier, T.; Luepschen, H.; Karsten, J.; Leibecke, T.; Großherr, M.; Gehring, H.; Leonhardt, S. Assessment of Regional Lung Recruitment and Derecruitment during a PEEP Trial Based on Electrical Impedance Tomography. Intensive Care Med. 2008, 34, 543–550. [CrossRef]

[70]. Zick, G.; Elke, G.; Becher, T.; Schädler, D.; Pulletz, S.; Freitag-Wolf, S.; Weiler, N.; Frerichs, I. Effect of PEEP and Tidal Volume on Ventilation Distribution and End-Expiratory Lung Volume: A Prospective Experimental Animal and Pilot Clinical Study. PLoS ONE 2013, 8, e72675. [CrossRef]

[71]. Odenstedt, H.; Lindgren, S.; Olegård, C.; Erlandsson, K.; Lethvall, S.; Åneman, A.; Stenqvist, O.; Lundin, S. Slow Moderate Pressure Recruitment Maneuver Minimizes Negative Circulatory and Lung Mechanic Side Effects: Evaluation of Recruitment Maneuvers Using Electric Impedance Tomography. Intensive Care Med. 2005, 31, 1706–1714. [CrossRef] [PubMed]

[72]. Van Heerde, M.; Roubik, K.; Kopelent, V.; Kneyber, M.C.J.; Markhorst, D.G. Spontaneous Breathing during High-Frequency Oscillatory Ventilation Improves Regional Lung Characteristics in Experimental Lung Injury. Acta Anaesthesiol. Scand. 2010, 54, 1248–1256. [CrossRef] [PubMed]

[73]. Costa, E.L.V.; Chaves, C.N.; Gomes, S.; Beraldo, M.A.; Volpe, M.S.; Tucci, M.R.; Schettino, I.A.L.; Bohm, S.H.; Carvalho, C.R.R.; Tanaka, H.; et al. Real-Time Detection of Pneumothorax Using Electrical Impedance Tomography. Crit. Care Med. 2008, 36, 1230–1238. [CrossRef] [PubMed]

[74]. Frerichs, I.; Schiffmann, H.; Hahn, G.; Hellige, G. Non-Invasive Radiation-Free Monitoring of Regional Lung Ventilation in Critically Ill Infants. Intensive Care Med. 2001, 27, 1385–1394. [CrossRef] [PubMed]

[75]. Miedema, M.; De Jongh, F.H.; Frerichs, I.; Van Veenendaal, M.B.; Van Kaam, A.H. Changes in Lung Volume and Ventilation during Surfactant Treatment in Ventilated Preterm Infants. Am. J. Respir. Crit. Care Med. 2011, 184, 100–105. [CrossRef] [PubMed]

[76]. Van Veenendaal, M.B.; Miedema, M.; De Jongh, F.H.C.; Van Der Lee, J.H.; Frerichs, I.; Van Kaam, A.H. Effect of Closed Endotracheal Suction in High-Frequency Ventilated Premature Infants Measured with Electrical Impedance Tomography. Intensive Care Med. 2009, 35, 2130–2134. [CrossRef]

[77]. Deibele, J.M.; Luepschen, H.; Leonhardt, S. Dynamic Separation of Pulmonary and Cardiac Changes in Electrical Impedance Tomography. Physiol. Meas. 2008, 29, S1–S14. [CrossRef]

[78]. Frerichs, I.; Hinz, J.; Herrmann, P.; Weisser, G.; Hahn, G.; Quintel, M.; Hellige, G. Regional Lung Perfusion as Determined by Electrical Impedance Tomography in Comparison with Electron Beam CT Imaging. IEEE Trans. Med. Imaging 2002, 21, 646–652. [CrossRef]

[79]. Shono, A.; Kotani, T.; Frerichs, I. Personalisation of Therapies in COVID-19 Associated Acute Respiratory Distress Syndrome, Using Electrical Impedance Tomography. J. Crit. Care Med. 2021, 7, 62–66. [CrossRef]

[80]. Mauri, T.; Spinelli, E.; Scotti, E.; Colussi, G.; Basile, M.C.; Crotti, S.; Tubiolo, D.; Tagliabue, P.; Zanella, A.; Grasselli, G.; et al. Potential for Lung Recruitment and Ventilation-Perfusion Mismatch in Patients with the Acute Respiratory Distress Syndrome from Coronavirus Disease 2019. Crit. Care Med. 2020, 48, 1129–1134. [CrossRef]

[81]. Pulletz, S.; Van Genderingen, H.R.; Schmitz, G.; Zick, G.; Schädler, D.; Scholz, J.; Weiler, N.; Frerichs, I. Comparison of Different Methods to Define Regions of Interest for Evaluation of Regional Lung Ventilation by EIT. Physiol. Meas. 2006, 27, S115–S127. [CrossRef] [PubMed]

[82]. Borgmann, S.; Linz, K.; Braun, C.; Dzierzawski, P.; Spassov, S.; Wenzel, C.; Schumann, S. Lung Area Estimation Using Functional Tidal Electrical Impedance Variation Images and Active Contouring. Physiol. Meas. 2022, 43, 075010. [CrossRef] [PubMed]

[83]. Ke, X.Y.; Hou, W.; Huang, Q.; Hou, X.; Bao, X.Y.; Kong, W.X.; Li, C.X.; Qiu, Y.Q.; Hu, S.Y.; Dong, L.H. Advances in Electrical Impedance Tomography-Based Brain Imaging. Mil. Med. Res. 2022, 9, 10. [CrossRef]

[84]. Hannan, S.; Faulkner, M.; Aristovich, K.; Avery, J.; Walker, M.; Holder, D. Imaging Fast Electrical Activity in the Brain during Ictal Epileptiform Discharges with Electrical Impedance Tomography. NeuroImage Clin. 2018, 20, 674–684. [CrossRef]

[85]. Hannan, S.; Faulkner, M.; Aristovich, K.; Avery, J.; Walker, M.C.; Holder, D.S. In Vivo Imaging of Deep Neural Activity from the Cortical Surface during Hippocampal Epileptiform Events in the Rat Brain Using Electrical Impedance Tomography. Neuroimage 2020, 209, 116525. [CrossRef] [PubMed]

[86]. Holder, D.S. Detection of Cortical Spreading Depression in the Anaesthetised Rat by Impedance Measurement with Scalp Electrodes: Implications for Non-Invasive Imaging of the Brain with Electrical Impedance Tomography. Clin. Phys. Physiol. Meas. 1992, 13, 77–86. [CrossRef] [PubMed]

[87]. Boverman, G.; Kao, T.J.; Wang, X.; Ashe, J.M.; Davenport, D.M.; Amm, B.C. Detection of Small Bleeds in the Brain with Electrical Impedance Tomography. Physiol. Meas. 2016, 37, 727–750. [CrossRef]

[88]. Fu, F.; Li, B.; Dai, M.; Hu, S.J.; Li, X.; Xu, C.H.; Wang, B.; Yang, B.; Tang, M.X.; Dong, X.Z.; et al. Use of Electrical Impedance Tomography to Monitor Regional Cerebral Edema during Clinical Dehydration Treatment. PLoS ONE 2014, 9, e113202. [CrossRef] [PubMed]

[89]. Shi, Y.; Tian, Z.; Wang, M. Simultaneous Imaging of Intracerebral Hemorrhage and Secondary Ischemia with Electrical Impedance Tomography. In Proceedings of the 2021 IEEE International Conference on Consumer Electronics and Computer Engineering, ICCECE 2021, Guangzhou, China, 15–17 January 2021; pp. 723–726.

[90]. Ferraioli, F.; Formisano, A.; Martone, R. Effective Exploitation of Prior Information in Electrical Impedance Tomography for Thermal Monitoring of Hyperthermia Treatments. IEEE Trans. Magn. 2009, 45, 1554–1557. [CrossRef]

[91]. Bottiglieri, A.; Dunne, E.; McDermott, B.; Cavagnaro, M.; Porter, E.; Farina, L. Monitoring Microwave Thermal Ablation Using Electrical Impedance Tomography: An Experimental Feasibility Study. In Proceedings of the 14th European Conference on Antennas and Propagation, EuCAP 2020, Copenhagen, Denmark, 15–20 March 2020.

[92]. Kao, T.J.; Boverman, G.; Kim, B.S.; Isaacson, D.; Saulnier, G.J.; Newell, J.C.; Choi, M.H.; Moore, R.H.; Kopans, D.B. Regional Admittivity Spectra with Tomosynthesis Images for Breast Cancer Detection: Preliminary Patient Study. IEEE Trans. Med. Imaging 2008, 27, 1762–1768. [CrossRef]

[93]. Akhtari-Zavare, M.; Latiff, L.A. Electrical Impedance Tomography as a Primary Screening Technique for Breast Cancer Detection. Asian Pacific J. Cancer Prev. 2015, 16, 5595–5597. [CrossRef]

[94]. Mansouri, S.; Chabchoub, S.; Alharbi, Y.; Alshrouf, A. EIT 40-Electrodes Breast Cancer Detection and Screening. IEEJ Trans. Electr. Electron. Eng. 2022, 17, 1141–1147. [CrossRef]

[95]. Ma, G.; Soleimani, M. Spectral Capacitively Coupled Electrical Resistivity Tomography for Breast Cancer Detection. IEEE Access 2020, 8, 50900–50910. [CrossRef]

[96]. Braun, R.P.; Mangana, J.; Goldinger, S.; French, L.; Dummer, R.; Marghoob, A.A. Electrical Impedance Spectroscopy in Skin Cancer Diagnosis. Dermatol. Clin. 2017, 35, 489–493. [CrossRef]

[97]. Stojadinovic, A.; Fields, S.I.; Shriver, C.D.; Lenington, S.; Ginor, R.; Peoples, G.E.; Burch, H.B.; Peretz, T.; Freund, H.R.; Nissan, A. Electrical Impedance Scanning of Thyroid Nodules before Thyroid Surgery: A Prospective Study. Ann. Surg. Oncol. 2005, 12, 152–160. [CrossRef] [PubMed]

[98]. Laufer, S.; Ivorra, A.; Reuter, V.E.; Rubinsky, B.; Solomon, S.B. Electrical Impedance Characterization of Normal and Cancerous Human Hepatic Tissue. Physiol. Meas. 2010, 31, 995–1009. [CrossRef] [PubMed]

[99]. Das, L.; Das, S.; Chatterjee, J. Electrical Bioimpedance Analysis: A New Method in Cervical Cancer Screening. J. Med. Eng. 2015, 2015, 636075. [CrossRef]

[100]. Zuluaga-Gomez, J.; Zerhouni, N.; Al Masry, Z.; Devalland, C.; Varnier, C. A Survey of Breast Cancer Screening Techniques: Thermography and Electrical Impedance Tomography. J. Med. Eng. Technol. 2019, 43, 305–322. [CrossRef]

[101]. Pathiraja, A.A.; Pathiraja, A.A.; Weerakkody, R.A.; Weerakkody, R.A.; Von Roon, A.C.; Von Roon, A.C.; Ziprin, P.; Ziprin, P.; Bayford, R.; Bayford, R. The Clinical Application of Electrical Impedance

Technology in the Detection of Malignant Neoplasms: A Systematic Review. J. Transl. Med. 2020, 18, 227. [CrossRef]

[102]. Yang, D.; Gu, C.; Gu, Y.; Zhang, X.; Ge, D.; Zhang, Y.; Wang, N.; Zheng, X.; Wang, H.; Yang, L.; et al. Electrical Impedance Analysis for Lung Cancer: A Prospective, Multicenter, Blind Validation Study. Front. Oncol. 2022, 12, 3418. [CrossRef]

[103]. Ye, G.; Lim, K.H.; George, R.T.; Ybarra, G.A.; Joines, W.T.; Liu, Q.H. 3D EIT for Breast Cancer Imaging: System, Measurements, and Reconstruction. Microw. Opt. Technol. Lett. 2008, 50, 3261–3271. [CrossRef]

[104]. Hong, S.; Lee, J.; Bae, J.; Yoo, H.J. A 10.4 MW Electrical Impedance Tomography SoC for Portable Real-Time Lung Ventilation Monitoring System. IEEE J. Solid-State Circuits 2015, 50, 2501–2512. [CrossRef]

[105]. Murphy, E.K.; Skinner, J.; Martucci, M.; Rutkove, S.B.; Halter, R.J. Toward Electrical Impedance Tomography Coupled Ultrasound Imaging for Assessing Muscle Health. IEEE Trans. Med. Imaging 2019, 38, 1409–1419. [CrossRef]

[106]. Iqbal, S.M.A.; Mahgoub, I.; Du, E.; Leavitt, M.A.; Asghar, W. Advances in Healthcare Wearable Devices. npj Flex. Electron. 2021, 5, 9. [CrossRef]

[107]. Huang, J.J.; Hung, Y.H.; Wang, J.J.; Lin, B.S. Design of Wearable and Wireless Electrical Impedance Tomography System. Meas. J. Int. Meas. Confed. 2016, 78, 9–17. [CrossRef]

[108]. Rapin, M.; Braun, F.; Adler, A.; Wacker, J.; Frerichs, I.; Vogt, B.; Chetelat, O. Wearable Sensors for Frequency-Multiplexed EIT and Multilead ECG Data Acquisition. IEEE Trans. Biomed. Eng. 2019, 66, 810–820. [CrossRef]

[109]. Zlochiver, S.; Arad, M.; Radai, M.M.; Barak-Shinar, D.; Krief, H.; Engelman, T.; Ben-Yehuda, R.; Adunsky, A.; Abboud, S. A Portable Bio-Impedance System for Monitoring Lung Resistivity. Med. Eng. Phys. 2007, 29, 93–100. [CrossRef]

[110]. Wu, Y.; Jiang, D.; Duan, J.; Liu, X.; Bayford, R.; Demosthenous, A. Towards a High Accuracy Wearable Hand Gesture Recognition system Using EIT. In Proceedings of the IEEE International Symposium on Circuits and Systems, Florence, Italy, 27–30 May 2018; Volume 2018.

[111]. Lu, X.; Sun, S.; Liu, K.; Sun, J.; Xu, L. Development of a Wearable Gesture Recognition System Based on Two-Terminal Electrical Impedance Tomography. IEEE J. Biomed. Health Inform. 2022, 26, 2515–2523. [CrossRef]

[112]. Lee, M.H.; Jang, G.Y.; Kim, Y.E.; Yoo, P.J.; Wi, H.; Oh, T.I.; Woo, E.J. Portable Multi-Parameter Electrical Impedance Tomography for Sleep Apnea and Hypoventilation Monitoring: Feasibility Study. Physiol. Meas. 2018, 39, 124004. [CrossRef]

[113]. Aliverti, A. Wearable Technology: Role in Respiratory Health and Disease. Breathe 2017, 13, e27–e36. [CrossRef]

[114]. Angelucci, A.; Aliverti, A. Telemonitoring Systems for Respiratory Patients: Technological Aspects. Pulmonology 2020, 26, 221–232. [CrossRef] [PubMed]

ISSN: 2454-9665

[115]. Angelucci, A.; Cavicchioli, M.; Cintorrino, I.A.; Lauricella, G.; Rossi, C.; Strati, S.; Aliverti, A. Smart Textiles and Sensorized Garments for Physiological Monitoring: A Review of Available Solutions and Techniques. Sensors 2021, 21, 814. [CrossRef] [PubMed]

[116]. Hong, S.; Lee, J.; Yoo, H.J. Wearable Lung-Health Monitoring System with Electrical Impedance Tomography. In Proceedings of the Annual International Conference of the IEEE Engineering in Medicine and Biology Society, EMBC, Milan, Italy, 25–29 August 2015; Volume 2015, pp. 1707–1710.

[117]. Adler, A.; Grychtol, B.; Bayford, R. Why Is EIT so Hard, and What Are We Doing about It? Physiol. Meas. 2015, 36, 1067–1073. [CrossRef] [PubMed]